Standardized Radiation Shield Design Method: 2005 HZETRN

J.W. Wilson, R.K. Tripathi,
NASA Langley Research Center, Hampton, VA 23681

F.F. Badavi
Christopher Newport University, Newport News, VA 23607

F.A. Cucinotta
NASA Johnson Space Center, Houston, TX 77058

ABSTRACT

Research committed by the Langley Research Center through 1995 resulting in the HZETRN code provides the current basis for shield design methods according to NASA STD-3000 (2005). With this new prominence, the database, basic numerical procedures, and algorithms are being re-examined with new methods of verification and validation being implemented to capture a well defined algorithm for engineering design processes to be used in this early development phase of the Bush initiative. This process provides the methodology to transform the 1995 HZETRN research code into the 2005 HZETRN engineering code to be available for these early design processes. In this paper, we will review the basic derivations including new corrections to the codes to insure improved numerical stability and provide benchmarks for code verification.

INTRODUCTION

Improved spacecraft shield design requires early entry of radiation constraints into the design process to maximize performance and minimize costs. As a result, we have been investigating computational procedures to allow shield analysis starting with preliminary design concepts through high-fidelity final design models (Wilson et al. 2003)[1]. Of particular importance is the need to implement probabilistic models to account for design uncertainties (Wilson et al. 2004a)[2] in the context of optimal design processes (Qualls et al. 2003)[3]. These requirements need supporting tools with high computational efficiency to enable these design processes. Only the HZETRN code has so far been identified for this purpose within the NASA STD-3000 (2005)[4] document. As a result, Wilson et al. (2005a)[5] have prepared a review of past HZETRN code development, verification, and validation. Although there has been sporadic research to generalize this code over the last ten years, evaluation of code status among principal users demonstrated drift in the various code versions and databases. As a result of this renewed interest in HZETRN for future space systems design, there is now a systematic effort to advance, verify, and validate these codes in preparation to integrate them into engineering design processes. The present paper will describe the first few months of this renewed systematic effort.

As NASA's newly defined development spirals are now progressing, there is a need to identify a suitable code for the early spiral processes. We have chosen the 1995 HZETRN version for early spiral development, this code has had wide distribution and is largely the code used in the prior verification and validation processes described by Wilson et al. (2005a)[5]. However, an assessment of the 1995 HZETRN code status demands the re-evaluation of the computational procedures and databases to account for software and database drift over the last ten years and the inherent limitations of these prior computational procedures. In the present paper, we examine the basic derivations to identify oversights and improve solution stability and accuracy. We use both analytical and Monte Carlo benchmarks to both identify problems among various versions and will distribute these benchmarks with the code package to evaluate future compiler and platform dependent problems in addition to future drift for whatever reason. This revised 1995 HZETRN code, chronicled as the 2005 HZETRN, is recommended for standard practice in an interim time period until a new version incorporating more recent research on methods is defined, verified, and validated.

2005 HZETRN

The atomic and nuclear processes associated with space radiation occur over very short time scales

(microseconds) compared with the secular variations of the space environment allowing use of a time independent master equation represented by a steady-state Boltzmann description balancing gains and losses (Wilson et al. 1991)[6] of the particle fields (Galactic Cosmic Rays, GCR, and Solar Particle Events, SPE) interacting with the shield material (including the human tissues). The basic procedures for reducing this equation to a readily soluble numerical process will be reviewed and further developed in the context of the marching procedures of the 1995 HZETRN algorithm.

TRANSPORT THEORY

The specification of the interior environment within a spacecraft and evaluation of the effects on the astronaut is at the heart of the space radiation protection problem. The Langley Research Center has been developing such techniques and an in-depth presentation is given Wilson et al. (1991)[6] although considerable progress has been made since that publication. The relevant transport equations are the coupled linear Boltzmann equations for a closed convex domain (Fig. 1) derived on the basis of conservation principles for the flux density (particles/cm^2-sr-s-A-MeV) $\phi_j(\boldsymbol{x}, \boldsymbol{\Omega}, E)$ for particle type j as

$$\boldsymbol{\Omega}\bullet\boldsymbol{\nabla}\phi_j(\boldsymbol{x},\boldsymbol{\Omega},E)= \sum_k \int \sigma_{jk}(\boldsymbol{\Omega},\boldsymbol{\Omega}',E,E')\,\phi_k(\boldsymbol{x},\boldsymbol{\Omega}',E')\,d\boldsymbol{\Omega}'\,dE' - \sigma_j(E)\,\phi_j(\boldsymbol{x},\boldsymbol{\Omega},E) \qquad (1)$$

where $\sigma_j(E)$ and $\sigma_{jk}(\boldsymbol{\Omega},\boldsymbol{\Omega}',E,E')$ are the shield media macroscopic cross sections. The $\sigma_{jk}(\boldsymbol{\Omega},\boldsymbol{\Omega}',E,E')$ represent all those processes by which type k particles moving in direction $\boldsymbol{\Omega}'$ with energy E' produce a type j particle in direction $\boldsymbol{\Omega}$ with energy E *(including decay processes)*. Note that there may be several reactions that produce a particular product, and the appropriate cross sections for equation (1) are the inclusive ones. Exclusive processes are functions of the particle fields and may be included once the particle fields are known. Note, we will at times loosely refer to $\phi_j(\boldsymbol{x}, \boldsymbol{\Omega}, E)$ as either flux or fluence and the usage should be clear from the context. The time scale of the processes in equation (1) are at most on the order of microseconds while time scales of boundary conditions are on the order of minutes or longer leaving the resulting interior fields in equilibrium with the particles at the boundary.

The total cross section $\sigma_j(E)$ with the medium for each particle type is

$$\sigma_j(E) = \sigma_j^{at}(E) + \sigma_j^{el}(E) + \sigma_j^{r}(E) \qquad (2)$$

where the first term refers to collision with atomic electrons, the second term is for elastic scattering on the nucleus, and the third term describes nuclear reactions where we have ignored the minor nuclear inelastic processes (excited single particle states) except for low energy neutron collisions. The corresponding differential cross sections are similarly ordered. Many atomic collisions (~10^6) occur in a centimeter of ordinary matter, whereas ~10^3 nuclear coulomb elastic collisions occur per centimeter, while nuclear scattering and reactive collisions are separated by a fraction to many centimeters depending on energy and particle type. We include in the $\sigma_j^r(E)$ term the nuclear decay processes. Solution methods first use physical perturbations based on the ordering of the cross sections with the frequent atomic interactions as the first physical perturbation with special methods used for neutrons for which atomic cross sections are zero. The first physical perturbation to be treated is the highly directed atomic collisions with mean free paths on the order of micrometers as observed in nuclear emulsion. The usual approximation is the continuous slowing down approximation leading to well specified range-energy relations as shown in Fig. 2 but neglects the energy straggling that will be studied later in the present treatment (see also Wilson et al. 2002)[7]. The next term is the highly directed multiple

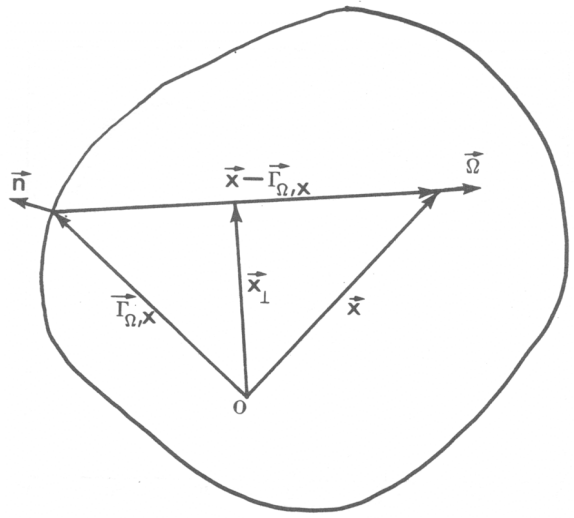

Fig. 1 Geometric relations of quantities useful in solving equation (1).

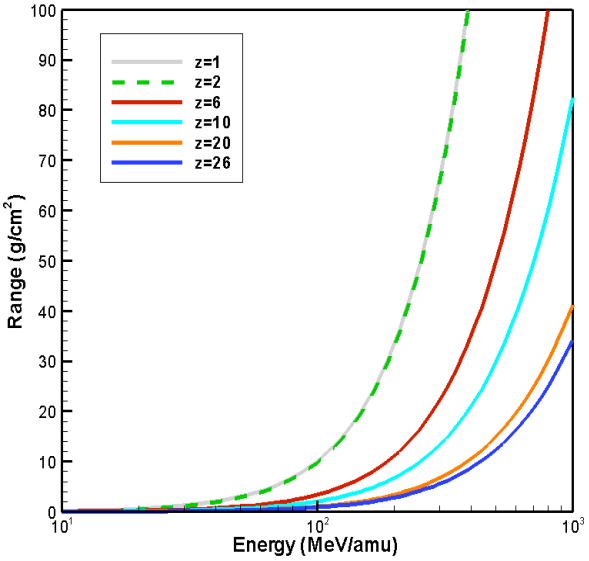

Fig. 2 Range of ions in aluminum.

coulomb scattering and is usually neglected in many models but is of great importance in understanding the transport of unidirectional ion beams leading to beam divergence and so is treated in detail elsewhere (Shavers et al. 1993)[8]. The remaining nuclear reactive processes have been given main attention in past code developments. We will now consider the formal development of the relevant equations for further consideration.

Continuous Slowing Down Approximation

The collisions with atomic electrons preserve the identity of the ion and the differential cross sections are given as

$$\sigma_{jk}^{at}(\boldsymbol{\Omega},\boldsymbol{\Omega}',E,E') = \Sigma_n \sigma_{j,n}^{at}(E')\,\delta(\boldsymbol{\Omega}-\boldsymbol{\Omega}')\,\delta_{jk} \times\delta(E + A_j^{-1}\varepsilon_n - E') \quad (3)$$

where n refers to the atomic/molecular excited states with excitation energies ε_n including the continuum. Note, the factor A_j^{-1} results from the units of E of A MeV (equivalent unit of MeV/nucleon). Although the atomic/molecular cross-sections $\sigma_{j,n}^{at}(E')$ are large ($\approx 10^{-16}$ cm^2), the energy transfers ε_n are small ($\approx$ 1-100 eV) compared to the particle energy. The atomic/molecular terms of equation (1) may be written as

$$\begin{aligned}&\Sigma\int \sigma_{jk}^{at}(\boldsymbol{\Omega},\boldsymbol{\Omega}',E,E')\,\phi_k(\mathbf{x},\boldsymbol{\Omega}',E')\,d\boldsymbol{\Omega}'\,dE' - \sigma_j^{at}(E)\,\phi_j(\mathbf{x},\boldsymbol{\Omega},E\\ &= \Sigma_n \sigma_{j,n}^{at}(E + A_j^{-1}\varepsilon_n)\,\phi_j(\mathbf{x},\boldsymbol{\Omega},E + A_j^{-1}\varepsilon_n) - \sigma_j^{at}(E)\,\phi_j(\mathbf{x},\boldsymbol{\Omega},E)\\ &= \Sigma_n \{\sigma_{j,n}^{at}(E)\,\phi_j(\mathbf{x},\boldsymbol{\Omega},E) + A_j^{-1}\varepsilon_n\,\partial_E[\sigma_{j,n}^{at}(E)\,\phi_j(\mathbf{x},\boldsymbol{\Omega},E)]\}\\ &\quad - \sigma_j^{at}(E)\,\phi_j(\mathbf{x},\boldsymbol{\Omega},E) + O(\varepsilon_n^2)\\ &= \partial_E[S_j(E)\,\phi_j(\mathbf{x},\boldsymbol{\Omega},E)] + O(\varepsilon_n^2) \quad (4)\end{aligned}$$

where the stopping power $S_j(E)$ is given as the sum of energy transfers and atomic excitation cross sections as

$$S_j(E) = \Sigma_n \varepsilon_n \sigma_{j,n}^{at}(E) \quad (5)$$

The higher order terms of equation (4) are neglected in the continuous slowing down approximation (csda) but are discussed elsewhere (Tweed et al. 2005)[9]. Evaluation of the stopping power by equation (5) is deceptively simple in that all of the excited states including continuum states of the atomic/molecular system need to be known. Furthermore, the projectile remains a bare ion except at low energies where the projectile ion atomic orbital states begin to resonate with the electrons of the media leading to electron capture and lowering of the ion charge. These issues are further discussed in Wilson et al. (1991)[6] and Tai et al. (1997)[10]. Equation (1) can be written in the csda as

$$\begin{aligned}&\boldsymbol{\Omega}\bullet\nabla\phi_j(\mathbf{x},\boldsymbol{\Omega},E) - A_j^{-1}\partial_E[S_j(E)\,\phi_j(\mathbf{x},\boldsymbol{\Omega},E)]\\ &= \Sigma\int \sigma_{jk}(\boldsymbol{\Omega},\boldsymbol{\Omega}',E,E')\,\phi_k(\mathbf{x},\boldsymbol{\Omega}',E')\,d\boldsymbol{\Omega}'\,dE'\\ &\quad - \sigma_j(E)\,\phi_j(\mathbf{x},\boldsymbol{\Omega},E) \quad (6)\end{aligned}$$

where the right-hand side of equation (6) excludes the atomic/molecular processes now appearing on the left as an energy shifting operator in addition to the usual drift term. Neutral particles would have null atomic cross sections for which the stopping term of equation (6) does not appear. Application of csda in both laboratory and space shielding has been wide and the resulting errors are discussed elsewhere (Tweed et al. 2005)[9]. Equation (6) can be rewritten as an integral equation (Wilson 1977)[11] as

$$\begin{aligned}&\phi_j(\mathbf{x},\boldsymbol{\Omega},E) = \{S_j(E_\gamma)P_j(E_\gamma)\,\phi_j(\boldsymbol{\Gamma}(\boldsymbol{\Omega},\mathbf{x}),\boldsymbol{\Omega},E_\gamma)\\ &\quad + \Sigma\int_E^{E_\gamma} dE'A_jP_j(E')\int_{E'}^{\infty}\int_{4\pi} dE''d\boldsymbol{\Omega}'\,\boldsymbol{\sigma}_{jr}(\boldsymbol{\Omega},\boldsymbol{\Omega}',E',E'')\\ &\quad \times\phi_k(\mathbf{x}+[R_j(E) - R_j(E')]\boldsymbol{\Omega},\boldsymbol{\Omega}',E'')\}/\,S_j(E)P_j(E) \quad (7)\end{aligned}$$

where $\boldsymbol{\Gamma}$ is the point on the boundary connected to $\mathbf{x}$ along $-\boldsymbol{\Omega}$, $E_\gamma = R_j^{-1}[\rho - d + R_j]$, ρ is the projection of $\mathbf{x}$ onto $\boldsymbol{\Omega}$ (Fig. 1), d is the projection of $\boldsymbol{\Gamma}$ onto $\boldsymbol{\Omega}$, $R_j(E)$ is the distance an ion of type j of energy E will travel before losing all of its energy to excitation of atomic electrons, and $P_j(E)$ is the probability a type j ion of energy E will have a nuclear reaction in coming to rest in the media. The usual range-energy relation is given (Fig. 2) by

$$R_j(E) = \int A_j\,dE'/S_j(E') \quad (8)$$

The nuclear attenuation function is given (Fig. 3) by

$$P_j(E) = \exp[-\int A_j\,\sigma_j(E')\,dE'/S_j(E')] \quad (9)$$

where the integral domains in equations (8) and (9) extend over the full energy range {0, E}.

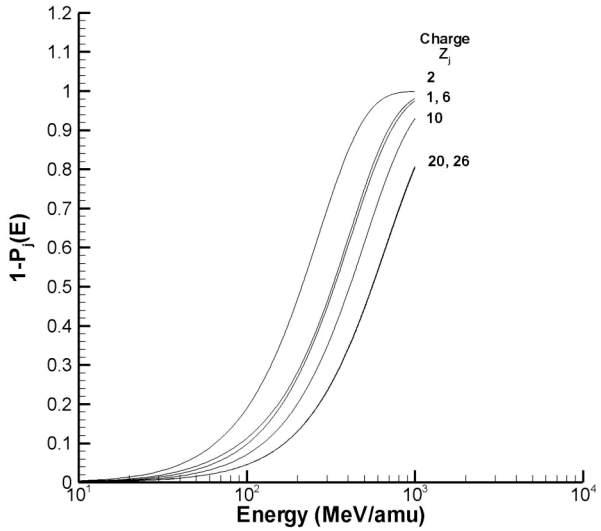

Fig. 3 Probability of nuclear reaction as a function of ion type and energy.

Straightahead Approximation

The approach to a practical solution of equation (7) is to develop a progression of solutions from the simple to the complex allowing early implementation of high-performance computational procedures and establishing a converging sequence of approximations with established accuracy criteria and means of verification. The lowest order approximation using the straightahead approximation was guided by the nucleon transport studies of Alsmiller et al. (1968)[12] using the Monte Carlo methods in which the differential cross sections were approximated as

$$\sigma^r_{jk}(\boldsymbol{\Omega},\boldsymbol{\Omega}',E,E') \approx \sigma^r_{jk}(E,E')\,\delta(\boldsymbol{\Omega}-\boldsymbol{\Omega}') \qquad (10)$$

resulting in dose and dose equivalent per unit fluence to be within the statistical uncertainty of the Monte Carlo result obtained using the fully angle dependent cross sections. The relation of angular dependent cross sections to spacecraft geometry in space application was further examined by Wilson and Kandelwal (1974)[13] using asymptotic expansions about angular divergence parameters demonstrating errors in the straightahead approximation to be on the order of the square of the ratio of distance of divergence to radius of curvature of the shield (a small error in most space systems).

Equations (6) and (7) were examined for HZE ions using the following form for the projectile fragmentation cross sections as

$$\sigma^r_{jk}(\boldsymbol{\Omega},\boldsymbol{\Omega}',E,E')= \sigma^r_{jk}(E')\,N_t\,\exp\{-[\boldsymbol{\Omega}\sqrt{E}-\boldsymbol{\Omega}'\sqrt{E'}]^2/2\,\varepsilon_{jk}^2\} \qquad (11)$$

where $\sigma^r_{jk}(E')$ is the cross section for producing fragment j from ion k, N_t is the normalization constant for the exponential function, and ε_{jk} is the momentum dispersion parameter in the reaction. Substituting the interactive form of equation (11) into the integral term (target fragments treated separately, Wilson 1977)[11] of the Boltzmann equation (6) yields

$$\begin{aligned}\sum\int \sigma^r_{jk}(\boldsymbol{\Omega},\boldsymbol{\Omega}',E,E')\,\phi_k(\mathbf{x},\boldsymbol{\Omega}',E')\,d\boldsymbol{\Omega}'\,dE' \\ = \sum \sigma^r_{jk}(E')\,\{\phi_k(\mathbf{x},\boldsymbol{\Omega},E) \\ + E\partial_E\,\phi_k(\mathbf{x},\boldsymbol{\Omega},E)\,\sqrt{[\varepsilon_{jk}^2/(2mE)]} \\ + \boldsymbol{\Omega}\bullet\boldsymbol{\partial}_{\boldsymbol{\Omega}}\,\phi_k(\mathbf{x},\boldsymbol{\Omega},E)\,\varepsilon_{jk}^2/(2mE)\}\end{aligned} \qquad (12)$$

where the second term on the right hand side of equation (12) results from corrections in assuming the velocity of the ion is preserved in the interaction (Curtis and Wilkinson, 1972, Wilson 1977)[14,11] and the third term is error resulting from the straightahead assumption (Alsmiller et al. 1968, Wilson 1977)[12,11]. The surprising result is that the velocity conserving assumption is inferior to the straightahead approximation for the nearly isotropic space radiation. Under approximations examined in equations (4) and (12) there are great simplifications in the Boltzmann equation as given below

$$\begin{aligned}\boldsymbol{\Omega}\bullet\boldsymbol{\nabla}\phi_j(\mathbf{x},\boldsymbol{\Omega},E) - A_j^{-1}\partial_E\,[S_j(E)\,\phi_j(\mathbf{x},\boldsymbol{\Omega},E)] \\ = \sum \sigma^r_{jk}(E)\,\phi_k(\mathbf{x},\boldsymbol{\Omega},E) - \sigma^r_j(E)\,\phi_j(\mathbf{x},\boldsymbol{\Omega},E)\end{aligned} \qquad (13)$$

which is strictly applicable to the HZE ions ($Z > 2$) and the light ions and neutrons have additional complications arising from the broad energy spectra associated with their production although the more favorable straightahead approximation is useful as indicated in equation (12) and as found by Alsmiller et al. (1967, 1968)[12,15] in their verification process. The corresponding light ion (and neutron) Boltzmann equation is

$$\begin{aligned}\boldsymbol{\Omega}\bullet\boldsymbol{\nabla}\phi_j(\mathbf{x},\boldsymbol{\Omega},E) - A_j^{-1}\partial_E\,[S_j(E)\,\phi_j(\mathbf{x},\boldsymbol{\Omega},E)] \\ = \sum\int \sigma^r_{jk}(E,E')\,\phi_k(\mathbf{x},\boldsymbol{\Omega},E')\,dE' - \sigma^r_j(E)\,\phi_j(\mathbf{x},\boldsymbol{\Omega},E)\end{aligned} \qquad (14)$$

where we have made use of the straightahead approximation as given by equation (10). Equations (13) and (14) have sufficient simplicity to allow an approach for both space and laboratory applications. The main force of the laboratory applications allow detailed model testing of the many atomic/molecular and nuclear processes.

Marching Procedures and HZETRN

The first version of the HEZTRN code is based on the solution of equation (14) as guided by the Monte Carlo studies of the straightahead approximation by Alsmiller et al. (1968)[12]. We again specialize to solution along a ray $\boldsymbol{\Omega}$ directed along the x-axis for which the Boltzmann equation becomes

$$[\partial_x - A_j^{-1}\partial_E S_j(E) + \sigma_j]\,\phi_j(x,E) = \Sigma_k\int \sigma_{jk}(E,E')\,\phi_k(x,E')\,dE' \qquad (15)$$

where $\sigma_{jk}(E,E')$ are approximated for nucleons by the multiplicities of Ranft (1980)[16], Bertini et al. (1972)[17], and quasi-elastic contribution as described by Wilson et al. (1991)[6]. An immediate problem is the near singular nature of the differential operator and transformation from energy to residual range coordinates as we did in developing the Green's function greatly relieves this problem (Wilson et al. 1991)[6]. Unlike the Green's function development, numerical procedures are simplified by introducing only a single residual range coordinate for all ions and the residual proton range r is used as the common coordinate as

$$r = \int_0^E dE'/S(E') \qquad (16)$$

and residual range of other particle types is related as $\nu_j\,r_j \approx r$ which fails at low energies corresponding to low residual range due to electron capture into atomic orbitals characteristic to each ion type. The corresponding transport equation is

$$\begin{aligned}[\partial_x - \nu_j\,\partial_r + \sigma_j(r)]\,\psi_j(x,r) \\ = \Sigma_k\int_r^\infty (\nu_j/\nu_k)\,s_{jk}(r,r')\,\psi_k(x,r')\,dr'\end{aligned} \qquad (17)$$

where scaled flux is now (ν_j for neutral particles such as neutrons are taken as unity in scaling relations, Wilson et al. 1991)[6]

$$\psi_j(x,r) = \nu_j\,S(E)\,\phi_j(x,E) \qquad (18)$$

and the scaled differential cross sections are

$$s_{jk}(r,r') = S(E)\,\sigma_{jk}(E,E') \qquad (19)$$

Errors in scaling of proton stopping and range parameters in arriving at the approximate transport equation (17) are compensated in part by solutions of equation (17) approaching a low energy equilibrium spectrum for ions given by

$$\nu_j\,S(E)\,\phi_j(x,E) \Rightarrow constant \qquad (20)$$

where the constant is fixed by the higher ion energy. In distinction, the solution to equation (15) for ions has the low energy equilibrium spectrum

$$A_j^{-1} S_j(E)\, \phi_j(x, E) \Rightarrow constant \qquad (21)$$

also fixed by the higher energy flux for which the range scaling relation $v_j\, r_j \approx r$ has better validity and the two constants are nearly equal so that equation (21) has improved accuracy over equation (20) at lower energies. This fact will require us to alter the flux unscaling relations as demanded by equation (21) to maintain accuracy at the lower energies. From equations (20) and (21), we can understand the simplicity of numerically solving equation (17) over numerical solution based on equation (15). The solution to equation (17) approaches a constant at small residual ranges allowing large separations in r grid values with smooth extrapolation to zero range whereas solutions of equation (15) vary as the nearly singular $1/S_j(E)$ for which small E grid spacing is required leading to slow computational procedures. We will test the assumptions in equation (17) and unscaling according to relation (21) later in this report.

The confusion caused by different scaling methods and associated coordinates for numerical procedures is justified by the simplification of the numerical representation of fluence of all particle types over a common residual range grid and simplification of the numerical procedures leading to high performance codes. Still a straightforward finite differencing of equation (17) can introduce unstable roots as had plagued the thermal transport problem for many years (Wilson et al. 1991)[6]. We will use the unconditionally stable methods of Wilson et al. (1991)[6] arrived at by inverting the differential operator (Wilson et al. 1977, 1989,1991)[11,18,6] of equation (7) as

$$\psi_j(x,r) = exp[-\zeta_j(r,x)]\, \psi_j(0, r + v_j\, x) + \Sigma_k \int_0^x \int_{r + v_j x'}^{\infty} exp[-\zeta_j(r,x')](\nu_j/\nu_k)\, s_{jk}(r + v_j\, x', r')\, \times \psi_k(x - x', r')\, dr'\, dx' \qquad (22)$$

where the exponential is the integrating factor related to attenuation of the j type ions with

$$\zeta_j(r,x) = \int_o^x \sigma_j(r + v_j\, x')\, dx' \qquad (23)$$

and is related to equation (9). Equation (22) is a Volterra equation and can be solved either as a Neumann series or with marching procedures. Note that the inverse mapping is taken as

$$\phi_j(x, E) = A_j\, \psi_j(x,r)/S_j(E) \qquad (24)$$

to guarantee the equilibrium solution given as equation (21) at low energies away from the boundaries (note, the proton stopping power is used in case of unscaling the neutron flux). We assume in this treatment that the equilibrium constant resulting from equation (22) and given in equation (20) differs little from condition (21) for which the inverse mapping of equation (24) is most accurate. We will be testing these approximations later in this report.

Two tracks are taken in implementing a marching procedure for equation (22) depending on particle type as demanded by the character of the nuclear processes. The problem naturally divides into "light ions" which will refer to all ions with atomic mass of four or less including neutrons and high charge-energy (HZE) ions have atomic mass greater than 4. The distinction arises from the energy and angle distributions of the double differential cross sections for which the HZE ions leaving a projectile fragmentation event have velocity nearly equal to that of the projectile as approximated by equation (11). Although the light ions are assumed to travel in the same direction as the projectile (see equation 10), they cover a broad energy distribution that cannot be ignored. The marching procedure is obtained by first considering equation (22) evaluated at $x + h$ where h is the step size. Clearly,

$$\psi_j(x+h,r) = exp[-\zeta_j(r,h)]\, \psi_j(x, r+v_j h) + \Sigma_k \int_0^h \int_{r + v_j x'}^{\infty} exp[-\zeta_j(r,x')](\nu_j/\nu_k)\, s_{jk}(r+v_j\, x', r')\, \times \psi_k(x+h-x', r')\, dr'\, dx' \qquad (25)$$

which may be used to develop a marching step from x to $x + h$ once a means to approximate the field function $\psi_j(x,r)$ across the subinterval $\{x, x+h\}$. If h is sufficiently small such that

$$\sigma_j(r)\, h << 1 \qquad (26)$$

then, following lowest order perturbation theory (Wilson and Lamkin 1975)[19], one has

$$\psi_k(x + h - x', r') = exp[-\zeta_k(r', h - x')]\, \psi_k[x, r' + v_k\, (h-x')] + O(h) \qquad (27)$$

which may be used to approximate the integral in equation (25) giving results for the fields $O(h^2)$ as required to control the propagated error (Wilson et al. 1991)[6]. Substituting equation (27) into (25) and evaluating the attenuation factors at the interval midpoint (mean value theorem) results in

$$\psi_j(x+h,r) = exp[-\zeta_j(r,h)]\, \psi_j(x, r+v_j\, h) + \Sigma_k\, exp[-\zeta_j(r,h/2) - \zeta_k(r', h/2)] \times \int_{r + v_j\, h/2}^{\infty} (\nu_j/\nu_k)\, F^{\Delta}_{jk}(h,r,r')\, \psi_k(x, r' + v_k\, h/2)]dr' + O(h^2) \qquad (28)$$

where the integrand has been simplified using

$$F^{\Delta}_{jk}(h,r,r') = \int_0^h s_{jk}(r + v_j\, x', r')\, dx' = F_{jk}(r + v_j\, h, r') - F_{jk}(r,r') \qquad (29)$$

and

$$F_{jk}(r,r') = \int_0^{\varepsilon(r)} \sigma_{jk}(E'', E')\, dE'' \qquad (30)$$

with $\varepsilon(r)$ the energy associated with proton residual range r, and $E' = \varepsilon(r')$. Note that if j corresponds to a neutral particle such as the neutron ($j = n$) then the above expressions are evaluated in the limit as v_j approaches zero in the range scaling relations resulting in the following (whereas the flux scaling factor for neutrons assumes $v_n = 1$)

$$\psi_n(x+h,r) = \exp[-\sigma_n(r)\,h]\,\psi_n(x,r) + \Sigma_{k\neq n}\exp[-\sigma_n(r)\,h/2 - \zeta_k(r',h/2)]\,h \times \int_r^\infty (1/\nu_k) s_{nk}(r,r')\,\psi_k(x, r'+\nu_k\,h/2)\,dr' + \exp[-\sigma_n(r)\,h/2 - \sigma_n(r')h/2]\,h \int_r^\infty s_{nn}(r,r')\,\psi_n(x,r')\,dr' \quad (31)$$

and similarly for the neutral k term ($k = n$) when the j particle is charged

$$\psi_j(x+h,r) = \exp[-\zeta_j(r,h)]\psi_j(x,r+\nu_j h) + \Sigma_{k\neq n}\exp[-\zeta_j(r,h/2) - \zeta_k(r',h/2)]\int_r^\infty(\nu_j/\nu_k)F^{\Delta}_{jk}(h,r,r'+\nu_j h/2) \times\psi_k[x, r'+(\nu_j+\nu_k)h/2)]\,dr' + \exp[-\zeta_j(r,h/2) - \sigma_n(r')\,h/2] \times \int_r^\infty \nu_j\,F^{\Delta}_{jn}(h,r,r'+\nu_j\,h/2)\,\psi_n(x, r'+\nu_j\,h/2)\,dr' \quad (32)$$

where ν_n in the flux scaling relation (24) is taken as unity. Equations (31) and (32) are solved on an equally space x-grid $\Delta x = h$ apart and a logarithmic spaced r-grid on two subintervals. The remaining integrals in these equations are approximated by (Wilson et al 1991)[6]

$$\int_{rk}^\infty K(r_n,r')\,\psi_j(x,r')\,dr' \approx \Sigma_{l=k}^\infty K[r_n,(r_l+r_{l+1})/2]\int_{rl}^{rl+1}\psi_j(x,r')\,dr' \quad (33)$$

where ∞ denotes a chosen upper limit tailored to the specific boundary condition. Note that the matrix of K-values can be evaluated once on the r-grid and stored for subsequent steps providing high computational efficiency. Equations (31) and (32) provide the basis of the light ion transport of both the HZETRN and the BRYNTRN codes. The HZE ion projectile ($A_j > 4$) coupling to the light fragments is contained in equations (28) to (32).

The HZE fragments are produced with nearly the same velocity as the projectile ion as expressed in equation (13) and results in the simplified Boltzmann equation as

$$[\partial_x - A_j^{-1}\partial_E S_j(E) + \sigma_j(E)]\,\phi_j(x,E) = \Sigma_k\,\sigma_{jk}(E)\,\phi_k(x,E) \quad (34)$$

for which the scaled equations result in contributions from all HZE ions (with $A_k > 4$) as

$$\psi_j(x,r) = \exp[-\zeta_j(r,x)]\,\psi_j(0,r+\nu_j\,x) + \Sigma_k\int_0^x \exp[-\zeta_j(r,x')](\nu_j/\nu_k) \times \sigma_{jk}(r+\nu_j\,x')\,\psi_k(x-x',r+\nu_j\,x')\,dx' \quad (35)$$

The corresponding marching equation (Wilson et al. 1991, Shinn et al. 1992)[6,20] is given as

$$\psi_j(x+h,r) = \exp[-\zeta_j(r,h)]\,\psi_j(x,r+\nu_j h) + \Sigma_k\int_0^h \exp[-\zeta_j(r,x')](\nu_j/\nu_k) \times \sigma_{jk}(r+\nu_j\,x')\,\psi_k(x+h-x',r+\nu_j x')\,dx' \quad (36)$$

for which the integrand can be approximated for sufficiently small h using

$$\psi_k(x+h-x',r+\nu_j x') = \exp[-\zeta_k(r+\nu_j x',h-x')] \times \psi_k[x, r+\nu_j x'+\nu_k\,(h-x')] + O(h) \quad (37)$$

allowing the following simplification

$$\psi_j(x+h,r) = \exp[-\zeta_j(r,h)]\,\psi_j(x,r+\nu_j h) + \Sigma_k\int_0^h \exp[-\zeta_j(r,x')-\zeta_k(r+\nu_j x',h-x')](\nu_j/\nu_k) \times \sigma_{jk}(r+\nu_j\,x')\,\psi_k[x, r+\nu_j x'+\nu_k\,(h-x')]\,dx' \quad (38)$$

To evaluate equation (38), we use the mean value theorem that guarantees linear terms of the final integral to be zero. First, we expand the attenuation factor as

$$\zeta_j(r,x') = \int_o^{x'}\sigma_j(r+\nu_j\,x'')\,dx'' \approx \int_o^{x'}[\sigma_j(r+\nu_j\,h/2) + \partial_r\sigma_j(r+\nu_j\,h/2)\,\nu_j\,(x''-h/2)]\,dx'' \quad (39)$$

and similarly for

$$\zeta_k(r+\nu_j x',h-x') = \int_o^{h-x'}\sigma_k[r+\nu_j\,x'+\nu_k\,(h-x'')]\,dx'' \approx \int_o^{h-x'}[\sigma_j(r+\nu_j\,x'+\nu_k\,h/2) + \partial_r\sigma_j(r+\nu_j\,x'+\nu_k\,h/2)\,\nu_k\,(x''-h/2)]\,dx'' \quad (40)$$

while applying the mean value theorem to the remaining factors of equation (38) and neglecting all but linear expansion terms in the integrand yields

$$\psi_j(x+h,r) = \exp[-\zeta_j(r,h)]\,\psi_j(x,r+\nu_j h) + \Sigma_k(\nu_j/\nu_k)\,\sigma_{jk}(r+\nu_j h/2)\,\psi_k[x, r+(\nu_j+\nu_k)h/2] \times\int_0^h \exp\{-\sigma_j(r+\nu_j h/2)x'-\sigma_k[r+(\nu_j+\nu_k)h/2)(h-x')]\}\,dx' = \exp[-\zeta_j(r,h)]\,\psi_j(x,r+\nu_j h) + \Sigma_k(\nu_j/\nu_k)\,\sigma_{jk}(r+\nu_j h/2)\,\psi_k[x, r+(\nu_j+\nu_k)h/2] \times[\exp\{-\sigma_j(r+\nu_j\,h/2)h\}-\exp\{-\sigma_k[r+(\nu_j+\nu_k)h/2)]h\}] /\{\sigma_k[r+(\nu_j+\nu_k)h/2)] - \sigma_j(r+\nu_j\,h/2)\} + O(h^2) \quad (41)$$

to be compared with the original HZETRN algorithm to $O[(\nu_j-\nu_k)h]$ derived by Shinn et al. (1992) given as

$$\psi_j(x+h,r) \approx \exp[-\zeta_j(r,h)]\,\psi_j(x,r+\nu_j h)+\Sigma_k(\nu_j/\nu_k)\sigma_{jk}(r) \times\psi_k(x,r+\nu_j h)\,\{\exp[-\sigma_j(r)h]-\exp[-\sigma_k(r)h]\}/[\sigma_k(r) - \sigma_j(r)] \quad (42)$$

In earlier versions of BRYNTRN for proton/neutron transport, the flux scaling relation was taken correctly as

$$\psi_j(x,r) = S(E)\,\phi_j(x,E) \quad (43)$$

but carried over to the final BRYNTRN for light-ions/neutron transport in the most recent version of BRYNTRN (Cucinotta 1993)[21]. In coupling to HZETRN with scaling given by

$$\psi_j(x,r) = \nu_j\,S(E)\,\phi_j(x,E) \quad (44)$$

there is an inconsistency in flux scaling which must be accounted. The appropriate coupling is given in equations (38) through (42) with the added factor of ν_j/ν_k in the field coupling terms. The main effects on solution of the Boltzmann equation are expected for the light ions of H^2, H^3, and He^3 with only minor effects on the major light-ion/neutron components (n, H^1, He^4). Note the main difference in the original and corrected code is determined by the ratios of ν_j/ν_k of the field coupling terms.

To evaluate these differences in flux scaling, we have used the algorithm of equations (31) thru (33) for comparison with the original light-ion/neutron propagator, we use the 29 September 1989 solar particle event spectrum because of its relation to the 23 February 1956 event (Wilson 2000)[22] represented by the proton spectrum (p/cm^2-MeV) at the boundary

approximated above 30 MeV by (Nymmik 1997, Cleghorn and Badhwar 1999)[23,24]

$$\phi_p(0, E) = (2.034\times10^7/\beta)\times[p(E)/p(30)]^{-4.5} \quad (45)$$

where $p(E)$ is the proton momentum (MV) given as

$$p(E) = \sqrt{[E(E + 1876)]} \quad (46)$$

and β is the proton speed relative to the speed of light. A low energy correction below 30 MeV mainly affecting transport results for depths less that 1 g/cm^2 in most materials is also added as

$$\phi_p(0, E) = 1.416\times10^8 \times exp[-p(E)/102.118] \times (E + 938)/p(E) \quad (47)$$

in good agreement with spectrometer data of the GOES satellite (Kim et al. 1999)[25]. The integral fluence values above 0.01 A MeV for neutrons, H^1, and He^4 with $\nu_j = 1$ are nearly unchanged (indistinguishable in Figs. 4-6) as they are the major components produced in reactions and H^1 is dominated by the fluence at the boundary over the first half of the mean free path. The H^2 and H^3 integral fluences are decreased according to their ν_j factors with values of *1/2* and *1/3* respectively (Figs. 7, 8). The He^3 integral fluence is increased by the factor of ν_j *=4/3* as seen in Fig. 9. It is expected that dose will change little as the excess of doubly charged He^3 contribution will largely cancel the singly charged H^2 and H^3 deficit contributions (approximately by a factor of (4/3 – 7/6) times the total minor contributor's dose).

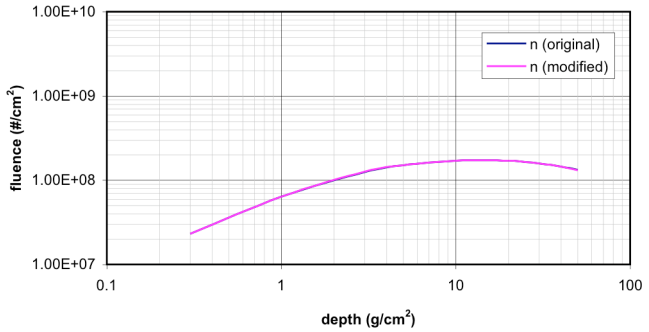

Fig. 4. Integral neutron fluence in aluminum shield using original and modified HZETRN code due to September 29, 1989 solar particle event.

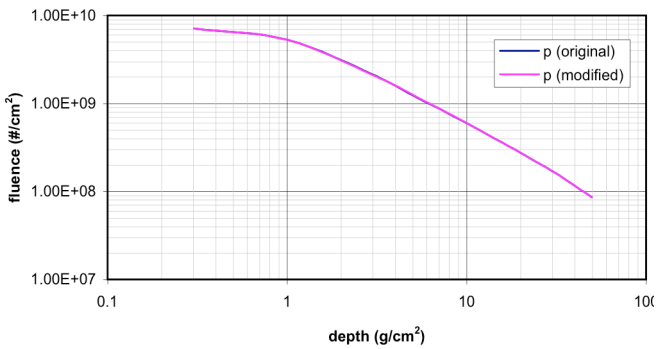

Fig. 5. Integral proton fluence in aluminum shield using original and modified HZETRN code for September 29, 1989 solar particle event.

The second correction to the propagator algorithm derived above, concerns the added accuracy of the HZE propagator to $O(h^2)$ in equation (41) as opposed to the original HZETRN with error term $O[(\nu_j-\nu_k)h]$. We will show that the improved HZE propagator of $O(h^2)$ allows control of the propagated error as well as reducing the local truncation error as we will demonstrate in the next section.

Numerical Analysis of Marching Procedures

There are two variables for which numerical approximation enter into the HZETRN propagator algorithms. The first is in the position variable x and the second is the residual range variable r. The coupling integrals of the Boltzmann equation involve integrals over energy that become principally integrals over residual range for the scaled flux equations although the energy shift operator of the Boltzmann equation couples residual range shift and position drift operators along the characteristic curves of the transport solution (Wilson 1977)[11]. The principal concern is the necessary control of local truncation errors to insure that propagated error is controlled. In consideration of how errors are propagated, the error introduced locally by evaluation of $\psi(x, r_i + h)$ over the range (energy) grid with which it is defined as

$$\psi(x + h, r_i) = exp(-\sigma h)\, \psi(x, r_i + h) \quad (48)$$

whereas the local truncation error is given by

$$\psi(x, r_i + h) = \psi_{int}(x, r_i + h) + \varepsilon_i(h, r_i) \quad (49)$$

After the k^{th} step from the boundary, the numerical solution is

$$\psi(kh, r_i) = exp(-\sigma h)\, \psi_{int}[(k-1)h, r_i + h] + \Sigma_{\lambda=0}^{k-1} exp[-\sigma(k - \lambda)h]\, \varepsilon_\lambda(h, r_i) \quad (50)$$

Suppose the local truncation error is bounded above such that $\varepsilon_\lambda(h,r_i) < \varepsilon(h)$ for all λ, then the propagated error is bounded by

$$\varepsilon_{prp}(h) = \Sigma_{\lambda=0}^{k-1} exp[-\sigma(k - \lambda)h]\, \varepsilon_\lambda(h) < \varepsilon(h) \Sigma_{\lambda=0}^{k-1} exp[-\sigma(k - \lambda)h] \approx \varepsilon(h)\, [1-exp(-\sigma kh)]/h\sigma \quad (51)$$

which is well behaved for all k and h if the local truncation error is bounded above by at least $O(h^2)$ as demonstrated by Wilson et al. many years ago (1991)[6]. The propagated error grows to a maximum of $\varepsilon(h)/h\sigma$ requiring the $O(h^2)$ limitation on the local error. The asymptotic bound for deep penetration is found to be

$$\varepsilon_{prp}(h) < \varepsilon(h)\, exp(-\sigma h)/[1- exp(-\sigma h)] \quad (52)$$

emphasizing again the need to control the local truncation error as $h\sigma \Rightarrow 0$. The original BRYNTRN and HZETRN propagator algorithms marginally met these requirements as was found by the detailed studies of Shinn et al. (1991, 1992)[20,26]. In the reductions leading to equations (31), (32) and (41), the error terms are $O(h^2)$ when the base algorithms are obtained but the

errors associated with the numerical approximation of the remaining functions of residual range (or energy) have been left so-far unspecified and were the subjects of prior studies (Shinn et al. 1991, 1992)[20,26] to be reviewed herein.

The original BRYNTRN and HZETRN codes assumed approximate log-linear dependence of all discretized field functions of residual range that are on $O(\Delta^2)$ for galactic cosmic ray like spectra where Δ is the order of the residual range spacing but only $O(\Delta)$ for most model solar particle events or trapped proton spectra (Wilson et al. 1991)[6].

The original range-grid was derived using a uniform log(E)-grid of thirty points converted to range using range-energy relations of the transport media. Detailed studies by Shinn et al. (1991)[26] used a 90-point log(E)-grid as standard for evaluation of errors in the original 30-point grid and a 60-point grid. Maximum errors were first quantified to be a few percent in dose and dose equivalent at the largest depths of 150 g/cm^2 in air (Tables 2&3 of Shinn et al. 1991)[26]. A systematic study of grid generation and numerical interpolation was then committed. It was found that a uniform log(r)-grid of 60-points gave an accurate interpolation (fraction of a percent of flux) with a fourth order Lagrange interpolation. It was desirable at that time to minimize the number of grid points as computational time is dominated by evaluation of the integral coupling terms and increases as N^2. It was clear in the studies of uniform log-grid spacing that only the midrange errors were significant so that Shinn et al. replaced the fully uniform grid with a uniform grid over two sub-domains allowing even greater accuracy with only 30 grid points. An excess number of points are over the range of 1 g/cm^2 with fewer points at the lower range values and is now a general feature of both BRYNTRN and HZETRN codes. The errors due to the residual range grid below 1 g/cm^2 has no effect on the propagated error as the step size is on the order of 1 g/cm^2 so that this low energy part of the spectrum is deposited in the sub-range of the next step. This is facilitated by the scaled flux that approaches a constant at these lower energies [see equations (20) and (21)].

Aside from the issue of numerical interpolation and direct effects on the propagation routines is the evaluation of integrals of field quantities related to coupling terms. The original BRYNTRN and HZETRN codes used the assumed log-linear dependence and evaluated quantities analytically arriving at computationally efficient procedures (an important feature on contemporary machines at that time). Shinn et al. (1991)[26] made detailed studies of numerical integration errors using the 90-point solutions as a standard for which the original algorithms for integral flux resulted in errors of less than 0.5 percent. It was found that substitution of a three-point Simpson's rule reduced the integration errors by

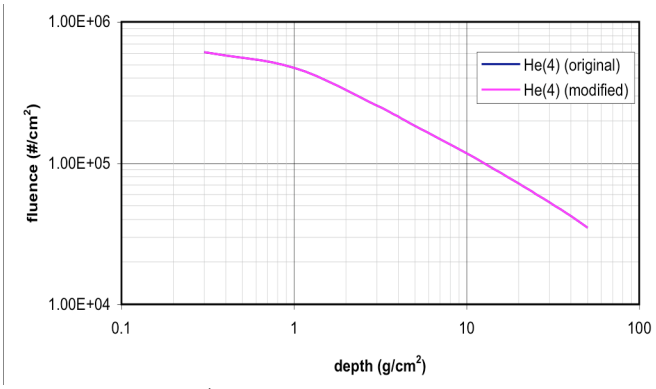

Fig. 6. Integral He^4 fluence in aluminum shield using original and modified HZETRN code for September 29, 1989 solar particle event.

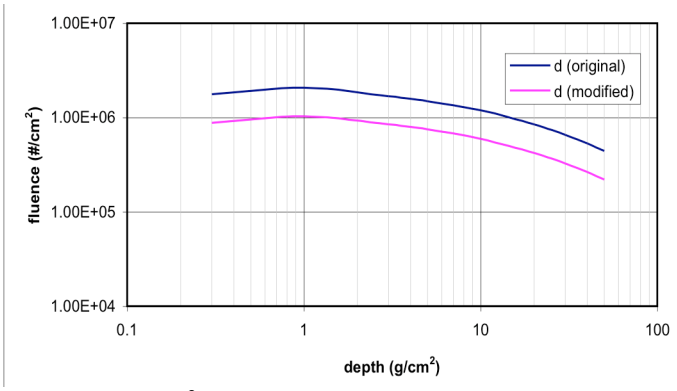

Fig. 7. Integral H^2 fluence in aluminum shield using original and modified HZETRN code for September 29, 1989 solar particle event.

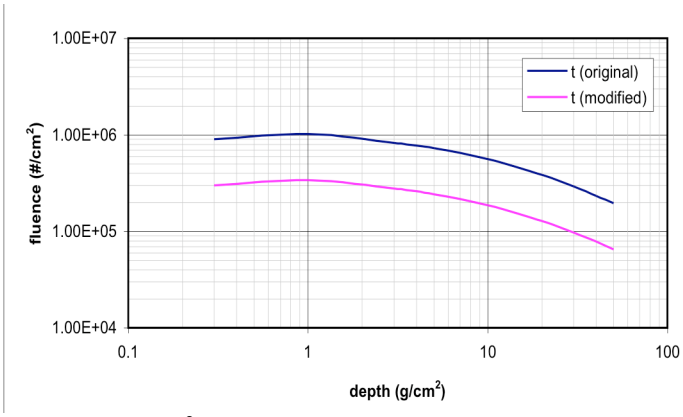

Fig.8. Integral H^3 fluence in aluminum shield using original and modified HZETRN code for September 29, 1989 solar particle event.

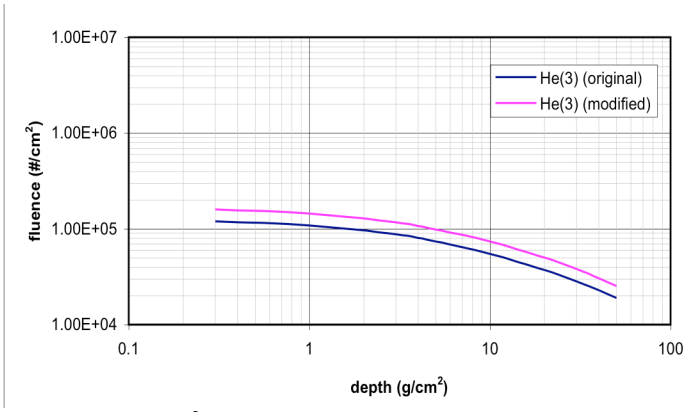

Fig.9. Integral He^3 fluence in aluminum shield using original and modified HZETRN code for September 29, 1989 solar particle event.

approximately an order of magnitude using midpoint values of the improved interpolation algorithm with the modified uniform log(r)-grid on two sub-domains. The reformulated propagation routines were found to have a fraction of percent error over the transport domain to 150 g/cm^2 depths. In every case so far studied, the approximations in equation (41) are assumed correct and attention is given to evaluation of the right hand side without reference to the original integral on the left side of equation (32). The adequacy of the approximation in equation (33) is being addressed in ongoing activities.

Shinn et al. (1991)[26] examined the step size convergence within the BRYNTRN algorithm using the aforementioned modifications with the 30-point converged results. The step size was varied from 1 g/cm^2 to 0.1 g/cm^2 for which dose for protons converged quickly but neutrons more slowly. The compromise step of 0.5 g/cm^2 is now standard in the BRYNTRN code and in the light ion propagator of HZETRN. The current version, so configured as discussed above with 30 log(r)-grid points, results in 5 percent accuracy to 150 g/cm^2 and is sufficient for most applications. Even so, standard practice now uses 80 such grid points assuring even improved accuracy for both GCR and SPE applications. Furthermore, the number of grid points is further adjusted to accommodate the simulation of geomagnetic cutoff effects while maintaining high numerical accuracy.

In addition to the improved numerical procedures, it is noted that the light-ion/neutron propagator of the 1995 HZETRN has substantial differences from its BRYNTRN

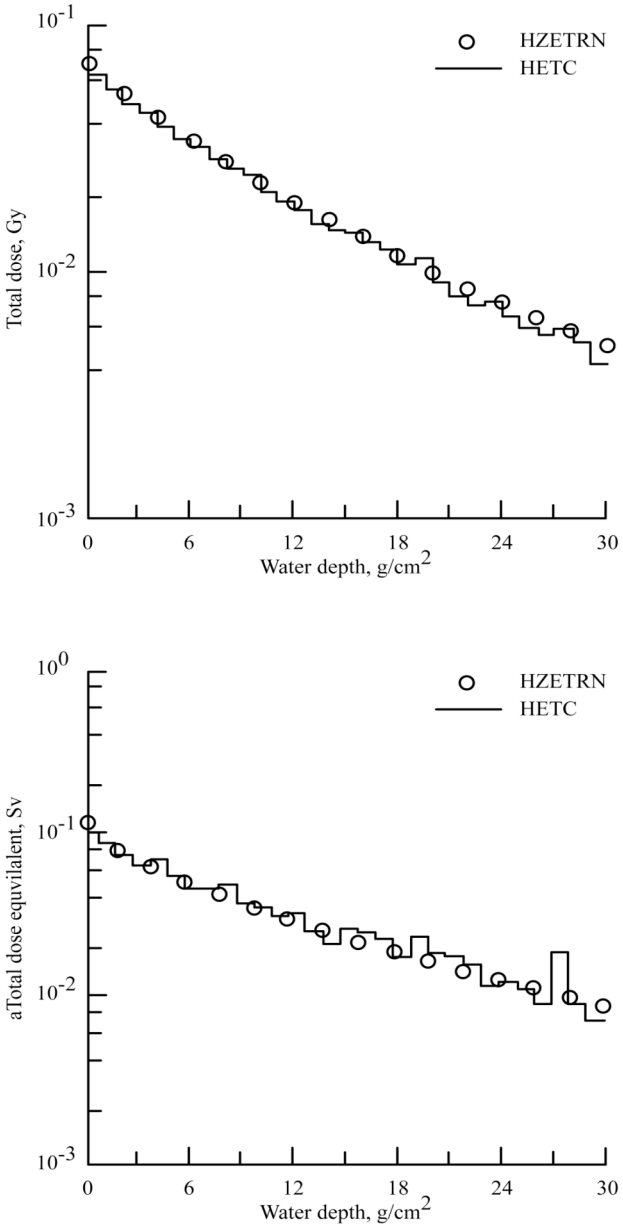

(a) Aluminum shield on water. 20 g/cm^2 A1; 30 g/cm^2 water.

Fig. 10. Total dose and dose equivalent (ICRP 26) for the Webber benchmark SPE spectrum.

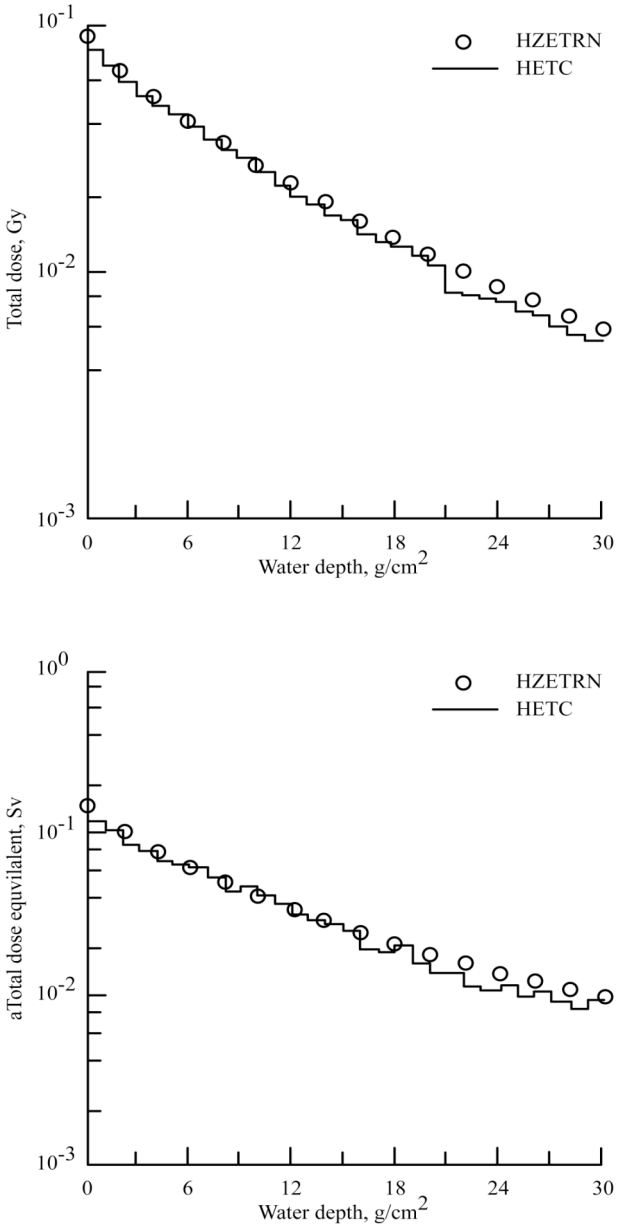

(b) Iron shield on water. 20 g/cm^2 Fe; 30 g/cm^2 water.

Fig. 10. Concluded.

(version 3) predecessor. To quantify these differences, we evaluate dose and dose equivalent (as given by both the ICRP 26 and ICRP 60 quality factors) in 30 cm of water behind a 20 g/cm^2 shield of aluminum (and alternately iron) for the Webber (1963)[27] approximation of the 23 February 1956 spectrum (p/cm^2-MeV) given as a P_0 = 100 MV spectrum with 10^9 protons /cm^2 above 30 MeV in the following

$$\phi_p(0, E) = 10^9 \times \exp\{[239.1 - p(E)]/100\} \times (2E + 1876)/[200 \times p(E)] \quad (53)$$

and comparing with the Monte Carlo results (an early version of HETC with ICRP 26 quality factors) of Scott and Alsmiller (1968)[28] and more modern Monte Carlo codes using ICRP 60 quality factors. We first re-evaluate the 2005 HZETRN version with the ICRP 26 quality factors by comparing to Scott and Alsmiller, the results are shown in Fig. 10 (a and b). A breakdown into specific contributions is presented by Wilson et al. (1991, 1995)[6,29] using an earlier version of BRYNTRN (version 1) and 1995 HZETRN, respectively.

We have further approached code testing with a benchmark by neglecting the integral term of equation (32) and boundary condition given by equation (53) in both the analytic solution and 1995 HZETRN code. The analytical solution is given in equation (35) neglecting the integral term and unscaling the result according to equation (24). The initial testing of the 1995 HZETRN version chosen at random from various copies revealed that the light-ion/neutron cross section routines were corrupted and we replaced them by more accurate (and uncorrupted) routines developed by Tripathi et al. (1998, 1999)[30,31]. Now the transported flux is generally within 1 percent of the analytic solution as is the dose using Simpson's rule but dose equivalent was found to be low by a few percent. Replacing Simpson's rule by a ten-point Gauss-Legendre quadrature brings dose equivalent to within 0.15 percent of the analytic result and Gauss-Legendre quadrature will be a permanent feature of the 2005 HZETRN code with comparisons in Table 1.

The percent differences of the analytical proton flux and the numerically generated proton flux at the iron-shield/water interface and at exit of the water slab are shown in Fig. 11. The results in Fig. 11 provide a direct test of the basic propagator methodology that is shown to be quite accurate. In addition to allowing evaluation of the accuracy of basic transport procedures and the nuclear attenuation factors, this benchmark provides a direct test of using equation (24) for unscaling the numerical solution developed on scaling relation (44) and demonstrating the requirements for the low energy equilibrium solution of equation (15) to be accurately maintained by the approximate numerical propagation method. The dose and dose equivalent at various depths in water for this analytic benchmark solution is given in Table 1. This benchmark solution is now a code feature useful for validation after porting to other platforms and differing compilers.

Table 1. Dose and dose equivalent (ICRP 60) of penetrating protons from analytical solution compared to numerical solution (in parenthesis). Webber spectrum on 20 g/cm^2 of iron shielding 30 cm water.

Depth, cm	Dose, cGy	Dose equivalent, cSv
0	8.405 (8.405)	11.520 (11.505)
5	4.083 (4.074)	5.009 (4.979)
10	2.321 (2.316)	2.817 (2.800)
15	1.417 (1.414)	1.707 (1.696)
20	0.909 (0.907)	1.089 (1.082)
25	0.604 (0.603)	0.720 (0.716)
30	0.412 (0.411)	0.490 (0.487)

* values in parenthesis are numerical solution

A similar analytic benchmark has been developed for the 1977 Solar minimum galactic cosmic ray spectrum and demonstrates that the propagator ignoring secondary particle production and fragmentation are a fraction of percent of the corresponding analytic solution with main errors near the boundaries of the energy grid as shown in Fig. 11 and most values are correct to a small fraction of 1 percent. The dose and dose equivalent of the analytic benchmark solution and numerical benchmark solution differ by less than 0.15 percent.

Benchmarking can be important in both evaluation the code accuracy as well as provision of test cases for code verification after porting to other platforms and/or compilers.

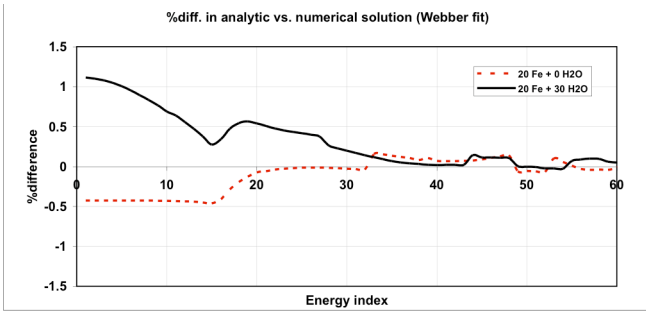

(a) analytic SPE benchmark

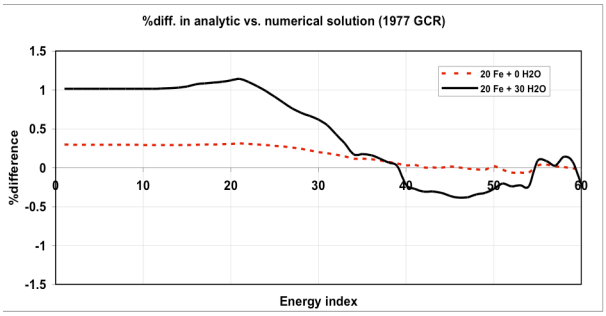

(b) analytic GCR benchmark

Fig. 11. Numerical errors in proton spectra for analytic (a) SPE and (b) GCR benchmarks versus energy index. Indexed energies for SPE range from 0.01 to 900 MeV and for GCR from 0.01 to 50,000 MeV.

The results of the BRYTRN (version 3), the 1995 HZETRN (including ten years of drift), and the 2005 HZETRN (improved numerical procedures as developed above) are shown in Fig. 12. There were many reasons for the differences including corruption of a nuclear reaction routine for light ions and a nuclear fragmentation database in addition to development of improved numerical procedures. We have made appropriate modifications as discussed above resulting in the 2005 HZETRN version with corrected nuclear routines and database. We have used a benchmark in the past based on an HETC result using the Webber spectrum for 30-cm slab of water shielded by 20 g/cm^2 iron (or aluminum) as shown in Fig. 10 for the 2005 HZETRN in comparison with dose and dose equivalent (ICRP 26 quality factor) according to HETC. It is clear that the result in Fig. 12 that considerable drift in codes have occurred over the years.

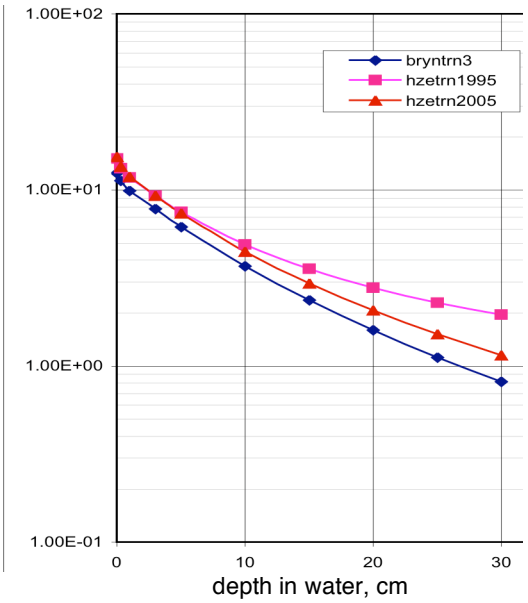

Fig. 12. Dose equivalent (ICRP 60) in water shielded from the Webber spectrum by 20 g/cm^2 of iron.

For future purposes, the dose and dose equivalent in water are given in Table 2 for 20 g/cm^2 shields of aluminum and iron at the end of this paper. Values for the 1977 Solar minimum GCR spectrum for the aluminum or iron shielded water are shown in Table 3. In these tables, values for dose, expected TLD100 response, and dose equivalent with ICRP 26 and ICRP 60 quality factors are given. Any future code usage should reproduce these tables to ensure that the codes have not accumulated additional software errors, platform errors, or compiler related errors.

Recently, new benchmarks have been provided for the two shield configurations described above (20 g/cm^2 of iron or aluminum shielding water) from the Monte Carlo Codes PHITS developed by the Japan Atomic Energy Agency (JAERI/JAEA)[32] and MULASSIS developed by the European Space Agency (ESA)[33]. The PHITS results are provided by Tatsuhiko Sato of JAEA and the MULASSIS results are provided by Jordi Bernabeu of Universitat Politècnica de Catalunya in collaboration with Hugh Evans of ESA/ESTEC. The Monte Carlo results for the Webber spectrum are shown in Table 4 to be compared with 2005 HZETRN results in Table 2. Dr. Sato also provided PHITS results for the 1977 Solar Minimum GCR spectrum given in Table 5. We note that differences between deterministic and Monte Carlo approaches tend to grow near the exit of the water column that may be caused by neutron (and lesser proton) leakage on the back surface that is not present in the current form of 2005 HZERN. There are other differences, especially for 1977 Solar Minimum GCR penetration problem, on the order of ten to twenty percent in dose and dose equivalent.

Future HZETRN Development

The next immediate step in code development is to validate this 2005 HZETRN using dosimetry and other instruments aboard shuttle and ISS for which improved dynamic/anisotropic environmental models have been recently derived (Wilson et al. 2005b)[34] In this activity, special emphasis will be given to validation and estimation of uncertainty similar to past activity (Wilson et al. 2005a)[5] Parallel to this validation activity is the development of the next generation engineering version of HZETRN with anticipated release in 2006.

Recent research activity associated with HZETRN has had two parallel tracks. The first track is to advance Green's function methods in anticipation of producing a code that is capable to be validated using high-energy ion beams (for example, Tweed et al. 2005).[35] The second track is to treat the off-axis scattering in the propagation of the light-ion/neutron propagator (Clowdsley et al. 2000, Heinbockel et al. 2003, Slaba et al 2006).[36,37,38] The next anticipated version of HZETRN will still use marching procedures for forward produced components of the interactions and evaluate the production source terms with broad angles with more appropriate angle dependent propagation techniques.

CONCLUSION

The reformulation of the HZETRN propagators with higher-order local truncation errors allows improved control of error propagation in the basic marching procedures. Conversion to dose and dose equivalent use improved numerical procedures based on a ten point Gauss-Legendre formulation. Analytical benchmarks are included in the 2005 HZETRN for code verification and in Table 1 of this report as a portable test. A benchmark with an early version of the HETC Monte Carlo code is contained herein in Fig. 10. A benchmark using the 2005 HZETRN code is given in Tables 2 and 3 for future verification on various platforms and/or compilers and to guard against drift in future

applications. Tables 4 and 5 contain new Monte Carlo benchmarks for evaluation of Tables 2 and 3 and for future reference.

ACKNOWLEDGMENTS

Our thanks to Tatsuhiko Sato, Japan Atomic Energy Research Institute, Tokai, Japan for the PHITS results and Jordi Bernabeu, Institute for Energy Techniques – Universitat Politècnica de Catalunya, Spain and Hugh Evans of ESA/ESTEC, The Netherlands for providing results from MULASSIS/GEANT4.

REFERENCES

1. Wilson, J.W., Korte, J.J., Sobieski, J., Badavi, F.F., Chokshi, S.M., Martinovic, Z.N., Cerro, J., Qualls, G.D. Radiation Shielding, MDO Processes, and Single Stage to Orbit Design. AIAA Space 2003 conference, AIAA 2003-6259.
2. Wilson, J.W., Cucinotta, F.A., Schimmerling, W. Emerging Radiation Health-Risk Mitigation Technologies. Space Technology Applications & Information Forum, STAIF-2004, AIP Conference Publications, 2004a.
3. Qualls, G.D., Wilson, J. W., Cucinotta, F.A., Nealy, J.E., Hugger, C.P., Atwell, W., and Shavers, M. International Space Station Radiation Shield Augmentation Optimization. Space 2003 Conference, AIAA 2003-6222.
4. NASA, *STD-3000, Vol. VIII, Human-Systems Integration Standards, Crew Exploration Vehicle Launch Segment.* http://www.exploration.nasa.gov /acquisition/cev_procurement.html
5. Wilson, J.W., Tripathi, R.K., Mertens, C.J., Blattnig, S.R., Clowdsley, M.S., Cucinotta, F.A., Tweed, J., Heinbockel, J.H., Walker, S.A., Nealy, J.E. *Verification and Validation: High Charge and Energy (HZE) Transport Codes and Future Development*. NASA/TP-213784, 2005a.
6. Wilson, J.W., Townsend, L.W., Schimmerling, W., Khandelwal, G.S., Khan, F., Nealy, J.E., Cucinotta, F.A., Simonsen; L.C., Shinn, J.L., Norbury, J.W. *Transport Methods and Interactions for Space Radiations*. NASA RP-1257, 1991.
7. Wilson, J.W., Tweed, J., Tai, H., and Tripathi, R.K. A simple model for straggling evaluation. *Nucl Inst & Methods* B 194: 389-392; 2002.
8. Shavers, M. R., Frankel, K., Miller, J., Schimmerling, W., Townsend, L. W., Wilson, J. W. The Fragmentation of 670 A MeV Neon-20 as a Function of Depth in Water. III. Analytic Multigeneration Transport Theory. *Radiat. Res.,* 134(1): 1-14; 1993.
9. Tweed, J., Walker, S.A., Wilson, J.W., Cucinotta, F.A., Tripathi, R.K., Blattnig, S., Mertens, C.J. Computational Methods for the HZETRN Code. *Adv. Space Res*. 35: 194-201; 2005.
10. Tai, H., Bichsel, H., Wilson, J. W., Shinn, J. L., Cucinotta, F. A., and Badavi, F. F. *Comparison of Stopping Power and Range Data Bases for Radiation Transport Study*. NASA TP-3644, 1997.
11. Wilson, J.W. *Analysis of the theory of high-energy ion transport*. NASA TN D-8381, 1977.
12. Alsmiller, R.G., Irving, D.C., Moran, H.S. Validity of the straightahead approximation in space-vehicle shielding studies. *Nucl. Sci. & Eng*. 32: 56-61; 1968.
13. Wilson, J.W., Khandelwal, G.S. Proton dose approximation in convex geometry. *Nucl. Tech*. 23: 298-305;1974.
14. Curtis, S.B., Wilkinson, M.C. The Heavy Particle Hazard—What Physical Data Are Needed? *Proceedings of the National Symposium on Natural and Manmade Radiation in Space,* E.A. Warman, ed., NASA TM-X2440, 1007-1015, 1972.
15. Alsmiller, R.G. High-Energy Nucleon Transport and Space Vehicle Shielding, *Nucl. Sci. & Eng*. 27: 158-189; 1967.
16. Ranft, J. The FLUKA and KASPRO Hadronic Cascade Codes. *Computer Techniques in Radiation Transport and Dosimetry,* W. R. Nelson and T.M. Jenkins, eds, Plenum Press, pp. 339-371, 1980.
17. Bertini, H.W.. Guthrie, M.P., Culkowski, A.H. *Nonelastic Interactions of Nucleons and π-Mesons with Complex Nuclei at Energies Below 3 GeV*. ORNL TM-3148, 1972.
18. Wilson, J.W., Lamkin, S.L., Farhat, H., Ganapol, Townsend, L.W. *A Hierarchy of Transport Approximations for High Energy Heavy Ion (HZE) Transport.* NASA TM-4118, 1989.
19. Wilson, J.W., Lamkin, S.L. Perturbation theory for charged-particle transport in one dimension. *Nuclear Sci & Eng.* 57:292-299; 1975.
20. Shinn, Judy L., John, Sarah, Tripathi, Ram K., Wilson, John W., Townsend, Lawrence W., and Norbury, John W. *Fully-Energy Dependent HZETRN (A Galactic Cosmic-Ray Transport Code).* NASA TP-3243, November 1992.
21. Cucinotta, F. A. *Calculations of cosmic ray helium transport in shielding materials*. NASA TP-3354, 1993.
22. Wilson, J.W. Overview of Radiation Environments and Human Exposures. *Health Physics* 79:470-494; 2000.
23. Nymmik, R.A., International Standard ISO WD 15391, 1997.
24. Cleghorn, T.T., Badhwar, G.D., Comparison of the SPE model with proton and heavy ion data. *Radiat. Meas*. 30:251-259; 1999.
25. Kim, M., Wilson, J.W., Cucinotta, F.A., Simonsen, L.C., Atwell, W., Badavi, F.F., Miller, J. *Contributions of High Charge and Energy (HZE) During Solar-Particle Event of September 29, 1989*. NASA/TP-1999-209320, 1999.
26. Shinn, J.L., John, S.; Wilson, J.W., Weyland, M., Cucinotta, F.A. *Improvements in Computational Accuracy of BRYNTRN (A Baryon Transport Code),* NASA TP-3093, May 1991.

27. Webber, W.R., *An Evaluation of the Radiation Hazard Due to Solar-Particle Events.* D2-90469, Aero-Space Div. The Boeing Co., 1963.
28. Scott, W.W., Alsmiller, R.G., *Comparison of Results Obtained with Several Proton Penetration Codes—Part II.* ORNL-RSIC-22, Oak Ridge National Laboratory, 1968.
29. Wilson, J. W., Badvi, F. F., Cucinotta, F. A., Shinn, J. L., Badhwar, G. D., Silberberg, R., Tsao, C. H., Townsend, L. W., and Tripathi, R. K. *HZETRN: Description of a Free-Space Transport and Shielding Program.* NASA TP-3495, May 1995.
30. Tripathi, R.K, Wilson, J.W., Cucinotta, F.A Nuclear Absorption Cross Sections using Medium Modified Nucleon-Nucleon Amplitudes. *Nuclear Instruments and Methods in Physics Research B (NIMB)*, Vol. 145, No. 3, pp. 277-282, 1998.
31. Tripathi, R.K, Cucinotta, F.A, Wilson, J.W. Medium Modified Nucleon-Nucleon Cross Sections in a Nucleus. *Nuclear Instruments and Methods in Physics Research B (NIMB)*, Vol. 152, pp. 425-431, 1999.
32. Iwase, H., Niita, K. and Nakamura, T. Development of a general-purpose particle and heavy ion transport Monte Carlo code. *J. Nuc. Sci. Technol.* 39(11): 1142-1151; 2002.
33. Lei, F., Truscott, R.R., Dyer, C.S., Quaghebeur, B., Heynderickx, D., Nieminen, R., Evans, H., Daly, E. MULASSIS: a Geant4-based multilayered shielding simulation tool, *Nuclear Science, IEEE Trans. on Nucl. Sci.* 49(6): 2788 – 2793; 2002.
34. Wilson, J.W., Cucinotta, F.A., Golightly, M.J., Nealy, J.E., Qualls, G.D., Badavi, F.F., de Angelis, G., Anderson, B.M., Clowdsley, M.S., Luetke, N., Zapp, N., Shavers, M.R., Semones, E., Hunter, A. International Space Station: A Testbed for Experimental and Computational Dosimetry. *Adv. Space Res.* (in press, 2005b).
35. Tweed, J., Walker, S.A., Wilson, J.W., Cucinotta, F.A., Tripathi, R.K., Blattnig, S., Mertens, C.J. Computational Methods for the HZETRN Code. *Adv. Space Res.* 35: 194-201; 2005.
36. Clowdsley, M.S., et al. A comparison of the multigroup and collocation methods for solving the low-energy neutron Boltzmann equation. *Can. J. Phys.* 78: 45-56; 2000.
37. Heinbockel, J.H., Feldman, G.D., Clowdsley, M.S., Wilson, J.W., Singleterry, R.C. Solutions to the Low Energy Neutron Boltzmann Equation. *International Conference on Environmental Systems.* SAE 2003-01-2339, 2003.
38. Slaba, T.C., Heinbockel, J.H., Wilson, J.W., Blattnig, S.R., Badavi, F.F. A New Method for Calculation of Low Energy Neutron Flux. *SAE ICES Conference*, Norfolk, 2006.

CONTACT

J.W. Wilson received his PhD from the College of William & Mary,1975. Email: john.w.wilson@nasa.gov. See Verified by a Netscape Security Partner: http://csmb.larc.nasa.gov/csmbexternal/Personnel/Wilson/wilsonbio.html

Table 2. Dose (cGy) and dose equivalent (cSv) in a 30 cm water slab protected by aluminum or iron shield from the Webber solar particle event spectrum.

Water Depth, cm	Aluminum Shield Thickness of 20 g/cm^2		Iron Shield Thickness of 20 g/cm^2	
x	D(x), cGy*	H(x), cSv**	D(x), cGy*	H(x), cSv**
0	7.09 (6.83)	11.86 (11.56)	9.18 (8.84)	15.39 (15.12)
5	3.86 (3.75)	6.06 (5.99)	4.68 (4.54)	7.32 (7.26)
10	2.36 (2.28)	3.84 (3.75)	2.77 (2.68)	4.45 (4.37)
15	1.53 (1.48)	2.53 (2.61)	1.77 (1.71)	2.95 (2.86)
20	1.04 (1.00)	1.85 (1.79)	1.18 (1.14)	2.07 (1.99)
25	0.74 (0.71)	1.40 (1.32)	0.83 (0.78)	1.52 (1.45)
30	0.54 (0.51)	1.08 (1.02)	0.60 (0.57)	1.16 (1.09)

*values in parenthesis are expected for TLD100, **values in parenthesis are for ICRP26 quality factors

Table 3. Annual dose (cGy) and dose equivalent (cSv) in a 30 cm water slab protected by aluminum or iron shield from the 1977 Solar Minimum GCR spectrum.

Water Depth, cm	Aluminum Shield Thickness of 20 g/cm^2		Iron Shield Thickness of 20 g/cm^2	
x	D(x), cGy*	H(x), cSv**	D(x), cGy*	H(x), cSv**
0	20.9 (18.9)	76.0 (66.8)	22.0 (19.7)	85.5 (75.7)
5	19.0 (17.5)	58.2 (51.7)	19.4 (17.8)	64.9 (57.5)
10	18.3 (17.0)	51.2 (45.8)	18.6 (17.3)	55.8 (49.8)
15	17.7 (16.6)	46.5 (41.9)	18.1 (16.8)	49.9 (44.7)
20	17.3 (16.2)	43.3 (41.8)	17.6 (16.4)	45.9 (41.3)
25	16.9 (15.9)	41.1 (37.2)	17.2 (16.1)	43.1 (39.9)
30	16.5 (15.5)	39.4 (35.7)	16.8 (15.8)	41.0 (37.1)

*values in parenthesis are expected for TLD100, **values in parenthesis are for ICRP26 quality factors

Table 4. Dose (cGy) and dose equivalent (cSv) in a 30-cm water slab protected by aluminum or iron shield from the Webber solar particle event spectrum evaluated using recent Monte Carlo codes: PHITS and MULASSIS/GEANT4 (within parenthesis).

Water Depth, cm	Aluminum Shield Thickness of 20 g/cm^2		Iron Shield Thickness of 20 g/cm^2	
x	D(x), cGy*	H(x), cSv*	D(x), cGy*	H(x), cSv*
0	7.09 (6.82±1.3%)	10.9 (10.67±3.3%)	9.21 (8.95±1.2%)	14.6 (14.12±2.8%)
5	3.90 (3.76±1.8%)	5.95 (5.62±4.8%)	4.74 (4.54±1.5%)	7.16 (6.55±3.2%)
10	2.37 (2.27±2.2%)	3.70 (3.48±7.2%)	2.79 (2.72±2.0%)	4.26 (4.14±6.5%)
15	1.53 (1.48±2.8%)	2.44 (2.14±6.3%)	1.76 (1.73±2.5%)	2.74 (2.56±6.8%)
20	1.03 (1.02±3.4%)	1.70 (1.62±8.3%)	1.17 (1.15±3.2%)	1.87 (1.80±8.9%)
25	0.717 (0.72±4.3%)	1.21 (1.05±7.0%)	0.806 (0.85±3.8%)	1.32 (1.33±14.5%)
30	0.511 (0.51±5.3%)	0.843 (0.87±18.3%)	0.565 (0.60±4.8%)	0.902 (0.94±9.9%)

*values in parenthesis are tentative GEANT4 results

Table 5. Annual dose (cGy) and dose equivalent (cSv) in a 30 cm water slab protected by aluminum or iron shield from the 1977 Solar Minimum GCR spectrum evaluated using the recent Monte Carlo code: PHITS

Water Depth, cm	Aluminum Shield Thickness of 20 g/cm^2		Iron Shield Thickness of 20 g/cm^2	
x	D(x), cGy	H(x), cSv	D(x), cGy	H(x), cSv
0	23.1	69.9	24.6	83.9
5	22.0	56.3	22.5	63.2
10	21.6	49.2	21.8	53.3
15	21.2	44.6	21.3	47.2
20	20.8	41.1	21.0	43.1
25	20.3	37.8	20.4	39.1
30	18.6	32.6	18.7	33.5